

1 **Localising individual atoms of tryptophan side chains in the metallo- β -lactamase IMP-1**
2 **by pseudocontact shifts from paramagnetic lanthanoid tags at multiple sites**

3 Henry W. Orton,^{a,*} Iresha D. Herath,^{b,*} Ansis Maleckis,^c Shereen Jabar,^b Monika Szabo,^d Bim
4 Graham,^d Colum Breen,^e Lydia Topping,^e Stephen J. Butler,^e Gottfried Otting^a

5
6 ^a ARC Centre of Excellence for Innovations in Peptide & Protein Science, Research School of
7 Chemistry, Australian National University, Canberra, ACT 2601, Australia

8 ^b Research School of Chemistry, The Australian National University, Sullivans Creek Road,
9 Canberra ACT 2601, Australia

10 ^c Latvian Institute of Organic Synthesis, Aizkraukles 21, LV-1006 Riga, Latvia

11 ^d Monash Institute of Pharmaceutical Sciences, Monash University, Parkville, VIC 3052,
12 Australia

13 ^e Department of Chemistry, Loughborough University, Epinal Way, Loughborough, LE11
14 3TU, United Kingdom

18

19 Correspondence: Gottfried Otting (gottfried.otting@anu.edu.au)

20 * These authors contributed equally to this work.

21

22 **Abstract**

23 The metallo- β -lactamase IMP-1 features a flexible loop near the active site that assumes
24 different conformations in single crystal structures, which may assist in substrate binding and
25 enzymatic activity. To probe the position of this loop, we labelled the tryptophan residues of
26 IMP-1 with $7\text{-}^{13}\text{C}$ -indole and the protein with lanthanoid tags at three different sites. The
27 magnetic susceptibility anisotropy ($\Delta\chi$) tensors were determined by measuring pseudocontact
28 shifts (PCS) of backbone amide protons. The $\Delta\chi$ tensors were subsequently used to identify
29 the atomic coordinates of the tryptophan side chains in the protein. The PCSs were sufficient
30 to determine the location of Trp28, which is located in the active site loop targeted by our
31 experiments, with high accuracy. Its average atomic coordinates showed barely significant
32 changes in response to the inhibitor captopril. It was found that localisation spaces could be
33 defined with better accuracy by including only the PCSs of a single paramagnetic lanthanoid
34 ion for each tag and tagging site. The effect was attributed to the shallow angle with which

35 PCS isosurfaces tend to intersect if generated by tags and tagging sites that are identical except
36 for the paramagnetic lanthanoid ion.

37

38 **1 Introduction**

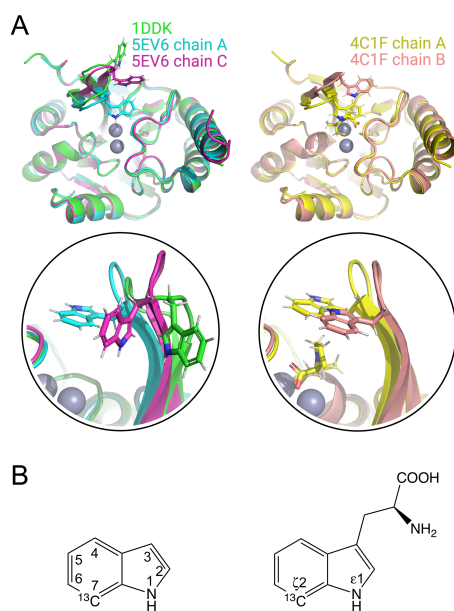
39 The metallo- β -lactamase IMP-1 is an enzyme that hydrolyses β -lactams, thus conferring
40 penicillin resistance to bacteria. First identified 30 years ago in the Gram-negative bacteria in
41 early 1990s from *Pseudomonas aeruginosa* and *Serratia marcescens* (Bush 2013), IMP-1 has
42 become a serious clinical problem due to horizontal gene transfer by a highly mobile gene
43 (*bla*_{IMP-1}) located on an integron (Arakawa et al., 1995), as the *bla*_{IMP-1} gene has been detected
44 in isolates of *Klebsiella pneumoniae*, *Pseudomonas putida*, *Alcaligenes xylosoxidans*,
45 *Acinetobacter junii*, *Providencia rettgeri*, *Acinetobacter baumannii* and *Enterobacter*
46 *aerogenes* (Ito et al., 1995; Laraki et al., 1999a; Watanabe et al., 1991). Critically, IMP-1
47 confers resistance also to recent generations of carbapenems and extended-spectrum
48 cephalosporins (Laraki et al., 199b; Bush et al., 2010; van Duin et al., 2013).

49 Multiple crystal structures have been solved of IMP-1, free and in complex with various
50 inhibitors (Concha et al., 2000; Toney et al., 2001; Moali et al., 2003; Hiraiwa et al., 2014;
51 Brem et al., 2016; Hinchliffe et al., 2016; 2018; Wachino et al., 2019; Rossi et al., 2021). IMP-
52 1 belongs to the subclass B1 of metallo- β -lactamases, which contain two zinc ions bridged by
53 the sulfur atom of a cysteine residue in the active site (Concha, 2000). One of Zn²⁺ ions can
54 readily be replaced by a Fe³⁺ ion (Carruthers et al., 2014). The active site is flanked by a loop
55 (referred to as L3 loop) that contains a highly solvent-exposed tryptophan residue surrounded
56 by glycine residues on either side. Both the loop and the tryptophan residue (Trp28 in the IMP-
57 1-specific numbering used by Concha et al. (2000) and Trp64 in the universal numbering
58 scheme by Galleni et al. (2001)) assume different conformations in different crystal structures,
59 suggesting that the loop acts as a mobile flap to cover bound substrate (Fig. 1A). The L3 loop
60 and the functional implication of its flexibility has been studied extensively for different
61 metallo- β -lactamases containing the Gly-Trp-Gly motif in the loop (Huntley et al., 2000; 2003;
62 Moali et al., 2003; Yamaguchi et al., 2015; Palacios et al., 2019; Gianquinto et al., 2020; Softley
63 et al., 2020). Flexibility of the L3 loop is a general feature also of many metallo- β -lactamases
64 without the Gly-Trp-Gly motif and is thought to contribute to the wide range of β -lactam
65 substrates that can be hydrolyzed by the enzymes (González et al., 2016; Linciano et al., 2019;
66 Salimraj et al., 2018). In the case of the metallo- β -lactamase from *B. fragilis*, which is closely
67 related to IMP-1, electron density could be detected for the Gly-Trp-Gly motif in the crystal

68 structure of the protein in the presence (Payne et al., 2003) but not absence of an inhibitor
69 (Concha et al., 1996), and an NMR relaxation study in solution confirmed the increased
70 flexibility of both the L3 loop and, in particular, the sidechain of the tryptophan residue
71 (Huntley et al., 2000). A similar situation prevails in the case of the IMP-1 variant IMP-13,
72 where different crystal structures of the ligand-free protein show the L3 loop in very different
73 conformations, sometimes lacking electron density, while NMR relaxation measurements
74 confirmed the increased flexibility of the loop (Softley et al., 2020).

75 Due to the rigidity of their sidechains, tryptophan residues frequently contribute to the
76 structural stability of three-dimensional protein folds and it is unusual to observe tryptophan
77 sidechains fully solvent-exposed as in the Gly-Trp-Gly motif of substrate-free IMP-1. The
78 functional role of Trp28 in IMP-1 was assessed in an early mutation study by mutating Trp28
79 to alanine and, in a different experiment, eliminating the L3 loop altogether. Enzymatic activity
80 measurements revealed an increase in the Michaelis constant K_m and a decrease in k_{cat}/K_m ratios
81 for all β -lactams tested, illustrating the importance of the Trp28 sidechain for catalytic activity.
82 Complete removal of the L3 loop reduced the k_{cat}/K_m ratios even further, but without
83 completely abolishing the enzymatic activity (Moali et al., 2003).

84
85



86

87 **Figure 1. Crystal structures of IMP-1 with different conformations of the loop L3 and chemical**
88 **structures of indole and tryptophan with atom names. (A)** Superimposition of crystal structures
89 of IMP-1 **highlighting** structural variations of Trp28 and the associated loop L3. The structures
90 shown are of the Zn²⁺/Zn²⁺ complex without inhibitor (green, PDB ID 1DDK, Concha et al.,
91 2000; cyan for chain A and magenta for chain C, PDB ID 5EV6, Hinchliffe et al., 2016), with
92 bound L-captopril (yellow for chain A and salmon for chain B, PDB ID 4CIF, Brem et al.,
93 2016). Zn²⁺ ions are represented by grey spheres and bound captopril is shown in the structure
94 4CIF chain A. **(B) Chemical structures of indole and tryptophan with selected ring positions**
95 **labelled according to IUPAC conventions. The present work used indole synthesised with a**
96 **¹³C-¹H group in position 7 and deuterium in the ring positions 2, 3, 4, 5 and 6 (Maleckis et al.,**
97 **2021).**

98
99 In the crystalline state, the conformation of a solvent-exposed loop is easily impacted
100 by crystal packing forces. Therefore, it is unclear what the actual conformation of the L3 loop
101 is in solution. To address this question, we used solution NMR spectroscopy to assess the
102 location of Trp28 in IMP-1 both in the absence and presence of the inhibitor L-captopril, which
103 inhibits metallo-β-lactamases by binding to the active-site zinc ions (Brem et al., 2016). The
104 analysis was hindered by incomplete backbone resonance assignments of IMP-1 attributed to
105 conformational exchange processes in parts of the protein (Carruthers et al., 2014). As it is
106 difficult to accurately position the atoms of a solvent-exposed polypeptide loop in solution by
107 nuclear Overhauser effects (NOE), we used pseudocontact shifts (PCS) generated by
108 lanthanoid ions attached at different sites of IMP-1 to determine the location of Trp28 relative
109 to the core of the protein. PCSs generated by multiple different paramagnetic metal ions or the
110 same metal ion attached at different sites of a protein have previously been shown to allow
111 localising atoms at remote sites of interest, such as in specific amino acid side chains (Pearce
112 et al., 2017; Lescanne et al., 2018), bound ligand molecules (Guan et al., 2013; Chen et al.,
113 2016) or proteins (Pintacuda et al., 2006; Keizers et al., 2010; de la Cruz et al., 2011;
114 Kobashigawa et al., 2012; Brewer et al., 2015) or for 3D structure determinations of proteins
115 (Yagi et al., 2013; Crick et al., 2015; Pilla et al., 2017).

116 IMP-1 contains six tryptophan residues, each containing several aromatic hydrogens
117 with similar chemical shifts. To increase the spectral resolution in the 2D NMR spectra
118 recorded for PCS measurements, we labelled each tryptophan sidechain with a single ¹³C atom
119 by expressing the protein in the presence of 7-¹³C-indole (Fig. 1B; Maleckis et al., 2021). The

Deleted: and chemical structures of indole and tryptophan. showing...

Formatted: Superscript

Formatted: Superscript

Deleted: z

123 results show that the localisation spaces defined by the tryptophan PCSs fully agree with
124 previously determined crystal structures of IMP-1 for all tryptophan residues. They suggest
125 little change in the average conformation of the L3 loop upon binding of captopril. The results
126 illustrate the accuracy with which the positions of individual atoms can be determined by PCSs
127 from lanthanoid tags even in proteins of limited stability.

129 2 Experimental procedures

130 2.1 Production, purification and tagging of proteins

131 2.1.1 Plasmid constructs and ¹³C-labelled indole

132 Three different cysteine mutations (A53C, N172C and S204C) were introduced into the *bla*_{IMP1}
133 gene in the pET-47b(+) plasmid using a modified QuikChange protocol (Qi and Otting, 2019).
134 Deuterated 7-¹³C-indole was synthesized as described with deuteration in all positions other
135 than position 7 (Maleckis et al., 2021). The amino acid sequence of the protein was that
136 reported in the crystal structure 4UAM (Carruthers et al., 2014), except that the N-terminal
137 alanine residue was substituted by a methionine to avoid heterogeneity by incomplete
138 processing by amino peptidase.

140 2.1.2 Protein production

141 Uniformly ¹⁵N-labelled samples of the cysteine mutants of IMP-1 were expressed in *E. coli*
142 BL21(DE3) cells. The cells were grown at 37 °C in Luria–Bertani (LB) medium containing 50
143 mgL⁻¹ kanamycin until the OD₆₀₀ reached 0.6–0.8 and were then transferred to 300 mL of M9
144 medium (6 gL⁻¹ Na₂HPO₄, 3 gL⁻¹ KH₂PO₄, 0.5 gL⁻¹ NaCl, pH 7.2) supplemented with 1 gL⁻¹
145 of ¹⁵NH₄Cl. After induction with isopropyl-β-D-thiogalactopyranoside (IPTG, final
146 concentration 1 mM), the cells were incubated at room temperature for 16 hours. Following
147 centrifugation, the cells were resuspended in buffer A (50 mM HEPES, pH 7.5, 100 μM ZnSO₄)
148 for lysis by a homogeniser (Avestin Emulsiflex C5). The supernatant of the centrifuged cell
149 lysate was loaded onto a 5 mL SP column, the column was washed with 20 column volumes
150 buffer B (same as buffer A but with 50 mM NaCl) and the protein was eluted with a gradient
151 of buffer C (same as buffer A but with 1 M NaCl).

152 IMP-1 samples containing 7-¹³C-tryptophan were produced by continuous exchange
153 cell-free protein synthesis (CFPS) from PCR-amplified DNA with eight-nucleotide single-
154 stranded overhangs as described (Wu et al., 2007), using 7-¹³C-indole as a precursor for the *in*
155 *vitro* production of tryptophan (Maleckis et al., 2021). The CFPS reactions were conducted at
156 30 °C for 16 h using 1 mL inner reaction mixture and 10 mL outer buffer. Tryptophan was

158 omitted from the mixture of amino acids provided and deuterated 7-¹³C-indole was added from
159 a stock solution in 50 % DMSO/50 % H₂O to the inner and outer buffers at a final concentration
160 of 0.75 mM. The protein samples were purified as described above. About 5 mg of the indole
161 was required for preparing each NMR sample.

Deleted: ~

163 2.1.3 Ligation with C2-Ln³⁺ tag

164 To ensure the reduced state of cysteine thiol groups, the protein samples were treated with 2
165 mM dithiothreitol (DTT) for 1 hour. Subsequently, the DTT was removed using an Amicon
166 ultrafiltration centrifugal tube with a molecular weight cut-off of 10 kDa, concentrating the
167 protein samples to 50 μM in buffer A. The samples were incubated overnight at room
168 temperature with shaking in the presence of five-fold molar excess of C2 tag (Graham et al.,
169 2011; de la Cruz et al., 2011) loaded with either Y³⁺, Tb³⁺ or Tm³⁺. Following the tagging
170 reaction, the samples were washed using an Amicon centrifugal filter unit to remove unbound
171 tag and the buffer was exchanged to NMR buffer (20 mM MES, pH 6.5, 100 mM NaCl).

173 2.1.4 Ligation with C12-Ln³⁺ tag

174 The ligation reaction of IMP-1 N172C with the C12-Ln³⁺ tag loaded with either Y³⁺, Tb³⁺ or
175 Tm³⁺ (Herath et al., 2021) was conducted in the same way as with the C2-Ln³⁺ tags, except that
176 the reactions were carried out in buffer A with the pH adjusted to 7.0.

178 2.2 NMR spectroscopy

179 All NMR data were acquired at 37 °C on Bruker 600 and 800 MHz NMR spectrometers
180 equipped with TCI cryoprobes designed for 5 mm NMR tubes, but only 3 mm NMR tubes were
181 used in this project. Protein concentrations were 0.6 mM and 0.2 mM for ¹⁵N-HSQC spectra
182 of samples labelled with the C2 and C12 tag, respectively. The protein concentrations were 0.4
183 mM for ¹³C-HSQC and NOE-relayed ¹³C-HSQC spectra. ¹⁵N-HSQC spectra were recorded at
184 a ¹H-NMR frequency of 800 MHz with $t_{1\max} = 40$ ms, $t_{2\max} = 170$ ms, using a total recording
185 time of 3 h per spectrum. ¹³C-HSQC spectra were recorded with a S³E filter to select the low-
186 field doublet component due to the ¹J_{HC} coupling of the ¹³C-labelled tryptophan side chains.
187 The pulse sequence is shown in Fig. S9 and the spectra were recorded at a ¹H-NMR frequency
188 of 600 MHz using $t_{1\max} = 20$ –50 ms, $t_{2\max} = 106$ ms and total recording times of 2 h per
189 spectrum. ¹³C-HSQC spectra with NOE relay were recorded without decoupling in the ¹³C-
190 dimension, relying on relaxation and ¹³C equilibrium magnetisation to emphasize the narrow

Deleted: 8

193 doublet component. The NOE mixing time was 150 ms and the total recording time 3 h per
194 spectrum. The pulse sequence is shown in Fig. S10.

195 To account for uncertainties in concentration measurements, samples with L-captopril
196 were prepared with a nominal ratio of captopril to protein of 1.5:1. In the case of samples
197 tagged with the C2 tag, however, this lead to gradual release of some of the tag, as captopril
198 contains a free thiol group and the disulfide linkage of the C2 tag is sensitive to chemical
199 reduction. To limit this mode of sample degradation, the NOE-relayed [¹³C,¹H]-HSQC spectra
200 were recorded with a smaller excess of captopril.

201

202 2.3 $\Delta\chi$ -tensor fits

203 The experimental PCSs ($\Delta\delta^{\text{PCS}}$) were measured in ppm as the amide proton chemical shift
204 observed in NMR spectra recorded for the IMP-1 mutants A53C, N172C and S204C tagged
205 with Tm³⁺ or Tb³⁺ tags minus the corresponding chemical shift measured of samples made with
206 Y³⁺ tags. The resonance assignments of the wild-type Zn₂ enzyme (BMRB entry 25063) were
207 used to assign the ¹⁵N-HSQC cross-peaks in the diamagnetic state. The program Paramagpy
208 (Orton et al., 2020) was used to fit magnetic susceptibility anisotropy ($\Delta\chi$) tensors to crystal
209 structures of IMP-1 solved in the absence and presence of the inhibitor captopril.

210

211 3 Results

212 3.1 Protein production

213 Three cysteine mutants of uniformly ¹⁵N-labelled IMP-1 were produced *in vivo*, where cysteine
214 residues replaced Ala53, Asn172 and Ser204, respectively. The purified proteins were tagged
215 with C2 tags containing Tb³⁺ or Tm³⁺ as the paramagnetic ions and Y³⁺ as the diamagnetic
216 reference. Samples of the uniformly ¹⁵N-labelled mutant N172C were also ligated with C12
217 tags containing the same set of metal ions. The chemical structures of the tags are depicted in
218 Fig. S1. To record ¹³C-¹H correlation spectra of the tryptophan side chains with minimal
219 spectral overlap, additional samples of the cysteine mutants were produced with selectively
220 ¹³C-labelled tryptophan residues. These samples were produced by cell-free protein synthesis
221 in the presence of 7-¹³C indole, deuterated except at the 7 position, with the omission of
222 tryptophan, using a recently established protocol (Maleckis et al., 2021). The residual activity
223 of tryptophan synthase in the cell-free extract was sufficient to produce tryptophan from the
224 added ¹³C-labelled indole. The resulting tryptophan residues contained a ¹³C-¹H group in
225 position 7 (¹³C^{ε2} and ¹H^{ε2} in IUPAC nomenclature; Markley et al., 1998) and deuterons at all

Deleted: 9

227 other hydrogen positions of the indole ring except for the H^N atom (H^{e1} in IUPAC
228 nomenclature). The cell-free expression yielded about 2 mg of purified protein per millilitre of
229 inner cell-free reaction mixture. Mass spectrometry indicated that the tryptophan residues of
230 IMP-1 were ¹³C/²H-labelled with about 80 % labelling efficiency at each of the six tryptophan
231 positions (Fig. S2). The purified proteins were ligated with C2-Ln³⁺ tags containing either Tb³⁺,
232 Tm³⁺ or Y³⁺ as in the case of the ¹⁵N-labelled samples. Ligation yields with the C2 tags were
233 practically complete as indicated by mass spectrometry (Fig. S2). The ligation yield of the
234 N172C mutant with C12 tags was about 90 % (Herath et al., 2021).

235

236 3.2 NMR experiments and resonance assignments

237 [¹⁵N,¹H]-HSQC spectra were measured of the tagged proteins in the free state and in the
238 presence of L-captopril (Fig. S3–S8). ¹H PCSs of backbone amide protons measured in these
239 spectra were used to establish the Δχ tensors relative to the protein. The resonance assignment
240 of the [¹⁵N,¹H]-HSQC spectra in the presence of inhibitor was transferred from the
241 corresponding spectra recorded in the absence of inhibitor. As no resonance assignments could
242 reliably be made in this way in areas of spectral overlap, fewer resonance assignments were
243 available in the presence than absence of inhibitor. Furthermore, due to captopril releasing
244 some of the C2 tags from the protein by breaking the disulfide bridge of the tag attachment,
245 spectra recorded in the presence of captopril contained additional cross-peaks from
246 diamagnetic protein.

247 To obtain tagged protein that is inert against chemical reduction, we also attached the
248 C12 tag to the mutant N172C. This tag, however, caused the appearance of additional peaks in
249 the [¹⁵N,¹H]-HSQC spectra (Fig. S7). The additional peaks appeared in different sample
250 preparations, indicating sample degradation or perturbation of the local protein structure by the
251 tag. We therefore based the rest of the work mainly on the PCSs obtained with the C2 tags.
252 Tables S1 and S2 list the PCSs of the backbone amides measured in the absence and presence
253 of captopril.

254 ¹H PCSs of the tryptophan H^{e2} protons were measured in [¹³C,¹H]-HSQC spectra
255 recorded with S³E spin-state selection element (Meissner et al., 1997) in the ¹³C dimension to
256 select the slowly relaxing components of the doublets split by ¹J_{HC} couplings. Cross-peaks were
257 observed for all six tryptophan residues except for the mutant N172C, which displayed cross-
258 peaks of only five tryptophan indoles (Fig. 2). The missing signal was attributed to Trp176
259 because of its close proximity to the tagging site. The indole H^{e1} proton is located within 2.9 Å

Deleted: 7

Deleted: 6

262 of the H^{ε2} proton and the NOE between both protons was readily observed in a [¹³C,¹H]-HSQC
263 experiment with NOE relay (Fig. 2). The H^{ε1} chemical shifts afforded better spectral resolution
264 than the H^{ε2} resonances. Comparison of the predicted and observed PCSs yielded resonance
265 assignments of all tryptophan H^{ε1} cross-peaks with particular clarity in the NOE-relayed
266 [¹³C,¹H]-HSQC spectrum (Fig. 2). In addition, the assignment was supported by paramagnetic
267 relaxation enhancements (for example, Trp88 is near residue 53 and therefore its cross-peaks
268 were strongly attenuated in the paramagnetic samples of the A53C mutant). Different PCSs
269 were observed for all six tryptophan sidechains and different PCSs were observed for the H^{ε2}
270 and H^{ε1} protons within the same indole sidechain. Each of the tryptophan sidechains showed
271 PCSs in most, if not all, of the mutants. As the L3 loop is near residue 172, the mutant N172C
272 endowed Trp28 with particularly large PCSs. Tables S3 and S4 report the PCSs measured in
273 this way for the samples labelled with C2 tags.

274 In contrast, assigning the indole N-H groups in the [¹⁵N,¹H]-HSQC spectra was much
275 more difficult because IMP-1 is a protein prone to showing more than a single peak per proton
276 (Figs S5 and S6). In particular, the [¹⁵N,¹H]-HSQC spectrum of wild-type IMP-1 selectively
277 labelled with ¹⁵N-tryptophan displayed six intense and at least three weak N^{ε1}-H^{ε1} cross-peaks
278 (Fig. S6; Carruthers *et al.*, 2014) and the [¹⁵N,¹H]-HSQC spectra of the tagged cysteine mutants
279 showed evidence of heterogeneity too (Fig. S5). Nonetheless, the six most intense N^{ε1}-H^{ε1}
280 cross-peaks could be assigned by comparison to the PCSs observed in the NOE-relayed
281 [¹³C,¹H]-HSQC spectrum and this assignment was used to measure the PCSs of the tryptophan
282 H^{ε1} resonances in the mutant N172C tagged with C12 tag (Fig. S8; Table S4).

283 Spectra recorded in the presence of L-captopril were very similar to those recorded
284 without the inhibitor, except that some new, narrow C-H cross-peaks appeared in the [¹³C,¹H]-
285 HSQC spectra of the mutants A53C and S204C, which were suggestive of protein degradation
286 (Fig. 3). We consequently used the better-resolved indole H^N cross-peaks to identify the correct
287 parent C-H cross-peaks. The chemical shifts of the tryptophan sidechains changed very little
288 in response to the presence of L-captopril, except for the ¹³C-chemical shift of Trp28, which is
289 nearest to the ligand binding site. The PCSs of the indole protons measured in the presence of
290 the inhibitor are listed in Tables S5 and S6.

291

292 3.2 Δχ-tensor fits

293 The Δχ-tensor parameters were determined using the program Paramagpy (Orton *et al.*, 2020),
294 using all available ¹H PCSs measured of backbone amides. Comparing the Δχ tensor fits to the

Deleted: .

Deleted: five

Deleted: five

Deleted: 7

299 crystal structures 5EV6 chains A and C (Hinchliffe et al., 2016) and 1DDK (Concha et al.,
300 2000) of the free protein, the chain A of the structure 5EV6 proved to produce the smallest Q
301 factor by a small margin (Fig. S11) and was used as the reference structure of the free protein
302 for the subsequent evaluation. Similarly, chain A of the co-crystal structure published with the
303 inhibitor L-captopril (PDB ID: 4C1F; Brem et al., 2016) on average delivered better fits than
304 chain B and was used as the reference structure for the NMR data recorded in the presence of
305 L-captopril. The $\Delta\chi$ -tensor fits of each mutant and tag used a common metal position for the
306 data obtained with the Tb^{3+} and Tm^{3+} tags. The fits positioned the paramagnetic centres at
307 distances between 8.2 and 9.4 Å from the $C\beta$ atom of the tagged cysteine residues, which is
308 compatible with the chemical structure of the C2-tag. Figure 4 shows the correlations between
309 back-calculated and experimental PCSs and Table S7 reports the fitted $\Delta\chi$ tensor parameters.
310 Very similar Q factors were obtained when using the PCSs measured in the absence of inhibitor
311 to fit the $\Delta\chi$ tensor to the co-crystal structure 4C1F or the PCSs measured in the presence of
312 inhibitor to fit the $\Delta\chi$ tensor to the crystal structure of the free protein. This indicates that the
313 protein structure did not change very much in response to inhibitor binding. This conclusion
314 was also indicated by the similarity between the backbone PCSs observed with and without
315 inhibitor (Fig. S12).

316 The $\Delta\chi$ tensors obtained with the Tb^{3+} tags were larger than those obtained with the
317 Tm^{3+} tags, which is also reflected by the consistently larger PCSs observed in the ^{13}C - 1H
318 correlation spectra of Fig. 2 and 3. The fits of $\Delta\chi$ tensors to the protein backbone also yielded
319 better Q factors for PCSs generated by Tb^{3+} than Tm^{3+} ions. Therefore, we determined the
320 localisation spaces of the tryptophan sidechains in the first instance by using their 1H PCSs
321 measured with Tb^{3+} tags only.

Deleted: 0

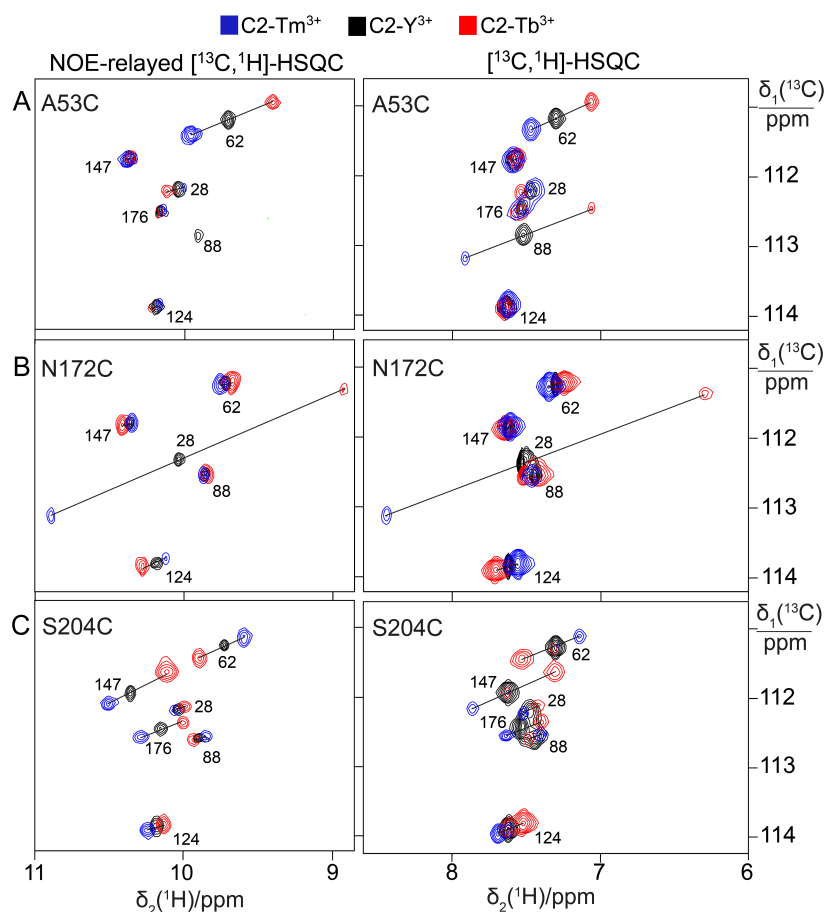
Deleted: 9

Deleted: 10.2

Deleted: α

Deleted: 1

Deleted: z



329
 330 **Figure 2.** PCSs observed in ^{13}C - ^1H correlation spectra of 0.4 mM solutions of IMP-1 mutants
 331 ~~tagged with C2-Ln $^{3+}$ tags and containing selectively isotope-labelled tryptophan produced from~~
 332 ~~7 - ^{13}C -indole deuterated in the positions 2, 4, 5 and 6.~~ The plots show superimpositions of
 333 spectra recorded with diamagnetic (C2-Y $^{3+}$, black) or paramagnetic (C2-Tb $^{3+}$, red; C2-Tm $^{3+}$,
 334 blue) tags. All spectra were recorded with spin-state selection in the ^{13}C -dimension to record
 335 the narrow low-field component of each ^{13}C -doublet. Right panels: ^{13}C , ^1H -HSQC spectra.
 336 Left panels: **NOE-relayed** ^{13}C , ^1H -HSQC spectra (150 ms NOE ~~mixing time~~) to record the H $^{\text{e1}}$
 337 resonances of the tryptophan side chains. PCSs are indicated by lines connecting the peaks of
 338 paramagnetic and diamagnetic samples. The cross-peaks are assigned with the residue number
 339 of the individual tryptophan residues. (A) Mutant A53C. (B) Mutant N172C. (C) Mutant

~~Deleted: labelled with 7 - ^{13}C -tryptophan (deuterated in the indole positions 2, 4, 5 and 6) and~~

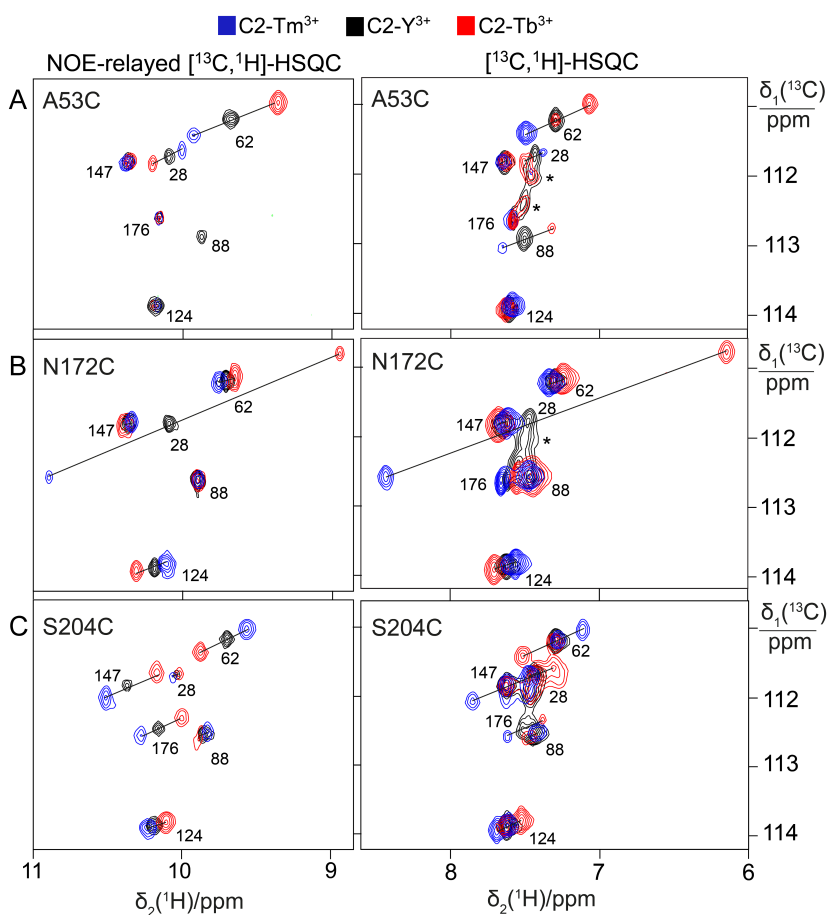
~~Deleted: .~~

~~Deleted: with~~

~~Deleted: relay~~

345 S204C.

346



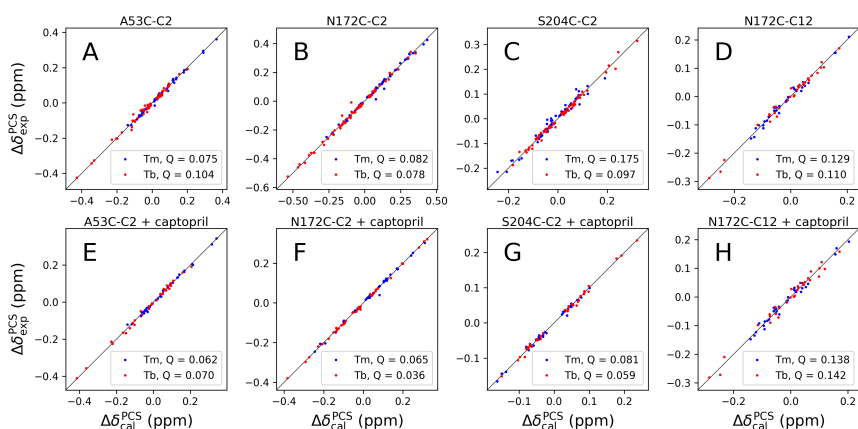
347

348 **Figure 3.** Effect of the presence of L-captopril on the PCSs observed in ^{13}C - ^1H correlation
349 spectra of 0.4 mM solutions of IMP-1 mutants. Protein preparations and experimental
350 parameters were the same as in Fig. 2. Spectra recorded with diamagnetic (C2- Y^{3+} , black) or
351 paramagnetic (C2- Tb^{3+} , red; C2- Tm^{3+} , blue) tags are superimposed. Right column: ^{13}C - ^1H -
352 HSQC spectra. Left column: NOE-related ^{13}C - ^1H -HSQC spectra recorded with 150 ms NOE
353 mixing time. Stars mark cross-peaks of species putatively attributed to protein degradation. (A)
354 Mutant A53C. (B) Mutant N172C. (C) Mutant S204C.

355

Deleted: recorded in

Deleted: with



358

359 **Figure 4.** Correlations between back-calculated and experimental ^1H PCSs measured of
 360 backbone amides of IMP-1 with C2 tags at three different sites (positions 53, 172 and 204) and
 361 the C12 tag in position 172. Red and blue data points correspond to the PCS data obtained with
 362 Tb^{3+} and Tm^{3+} tags, respectively. (A) Mutant A53C with C2 tag. (B) Mutant N172C with C2
 363 tag. (C) Mutant S204C with C2 tag. (D) Mutant N172C with C12 tag. (E) Same as (A) but in
 364 the presence of captopril. (F) Same as (B) but in the presence of captopril. (G) Same as (C) but
 365 in the presence of captopril. (H) Same as (D) but in the presence of captopril. PCS data in (A)–
 366 (D) were used to fit $\Delta\chi$ tensors to the structure 5EV6. PCS data in (E)–(F) were used to fit $\Delta\chi$
 367 tensors to the structure 4C1F.

368

369 3.3 Determining the localisation spaces of tryptophan sidechains

370 The $\Delta\chi$ tensors determined of backbone amides not only enabled the resonance assignment of
 371 the tryptophan sidechains by comparing back-calculated with experimental PCSs, but also
 372 allowed translation of the indole PCSs into restraints that define the locations of the tryptophan
 373 $\text{H}^{\zeta 2}$ and $\text{H}^{\epsilon 1}$ atoms with respect to the rest of the protein. The concept of localising nuclear spins
 374 by PCSs that are generated by lanthanoid tags at different sites is well-established (see, e.g.,
 375 Yagi et al., 2013; Lescanne et al., 2018; Zimmermann et al., 2019). It can be visualised by
 376 representing each PCS restraint by the corresponding PCS isosurface, which comprises all
 377 points in space where this PCS value is generated by the $\Delta\chi$ tensor (Fig. 5). With PCS restraints
 378 from two different metal sites, the intersection between the respective isosurfaces defines a
 379 line. The intersection of this line with the PCS isosurface from a third $\Delta\chi$ tensor defines two
 380 points. While a fourth $\Delta\chi$ tensor could unambiguously produce a single solution, a fourth tensor

381 may not be required if one of these two points is incompatible with the covalent structure of
382 the protein. In favourable circumstances, the constraints imposed by the covalent structure may
383 even allow the accurate positioning of nuclear spins by PCSs generated from only two different
384 $\Delta\chi$ tensors (Pearce et al., 2017). Therefore, the present study was successful with only three
385 different tagging sites. Figure S13 illustrates the concept for the Trp28 $H^{\epsilon 1}$ atom.

386 The spatial definition of the intersection point defined by the PCS isosurfaces depends
387 on the experimental uncertainties in a non-isotropic way, as the PCS isosurfaces rarely intersect
388 in an orthogonal manner and the PCS gradients differ for each $\Delta\chi$ tensor. To capture a
389 localisation space, which allows for the experimental uncertainty in the measured PCS data,
390 we mapped the spatial field of root-mean-squared deviations (RMSD) between experimental
391 and calculated PCS values and defined the boundary of the localisation space by a maximal
392 RMSD value. In addition, uncertainties in the $\Delta\chi$ tensors were propagated by averaging over
393 the results from 20 $\Delta\chi$ -tensor fits performed with random omission of 20 % of the backbone
394 PCS data. In the present work, the routine for defining the localisation space was implemented
395 as a script in the software Paramagpy (Orton et al., 2020). Figure 6 shows the resulting
396 localisation spaces for the $H^{\epsilon 1}$ and $H^{\epsilon 2}$ atoms of Trp28, using the PCS data obtained for the
397 three cysteine mutants A53C, N172C and S204C with the C2-Tb³⁺ tag as well as the N172C
398 mutant with the C12-Tb³⁺ tag.

399 The localisation spaces found for the $H^{\epsilon 1}$ and $H^{\epsilon 2}$ atoms of Trp28 were clearly different.
400 Furthermore, the distance between them corresponded closely to the distance expected from
401 the chemical structure of the indole ring (2.9 Å). The irregular shapes of the localisation spaces
402 displayed in Fig. 6 purely reflect the relative geometry of the intersecting PCS isosurfaces and
403 do not take into account any dynamic flexibility of the L3 loop or protein structure. In
404 particular, the relevant PCS isosurfaces associated with the C2 tag at sites N172C and S204C
405 intersect at a shallow angle, which leads to the elongated shape of the localisation space for the
406 Trp28 $H^{\epsilon 2}$ atom (Fig. S13). For the nitrogen-bound $H^{\epsilon 1}$ atom, the localisation space was
407 restricted further by the additional data obtained with the C12 tag at site N172C (Fig. 6).
408 Calculating the localisation spaces from the Tm³⁺ data yielded very similar results (Fig. S14).
409 The agreement of the localisation spaces of Trp28 with chain A of the previously published
410 crystal structure 5EV6 is excellent and they are clearly incompatible with the conformations
411 observed in chain C of the same structure or in the structure 1DDK (Fig. 1A).

412 Due to close proximity to the C2 tags in the N172C mutant, the largest PCSs were
413 observed for Trp28 $H^{\epsilon 1}$ but, in the absence of captopril, their exact magnitude appeared about

Deleted: 2

Deleted: 5

Deleted: 2

Deleted: 3

418 0.3 ppm smaller in the [¹⁵N,¹H]-HSQC (Fig. S5b) than the NOE-relayed [¹³C,¹H]-HSQC (Fig.
419 2B) spectrum. The centre of the localisation space of Trp28 H^{ε1} moved to a slightly more open
420 L3 loop conformation when using the smaller PCS detected in the [¹⁵N,¹H]-HSQC spectrum
421 of the N172C mutant labelled with the C2-Tb³⁺ tag. The space still encompassed the
422 coordinates observed in the structure 5EV6, limiting the significance of this difference in PCS.

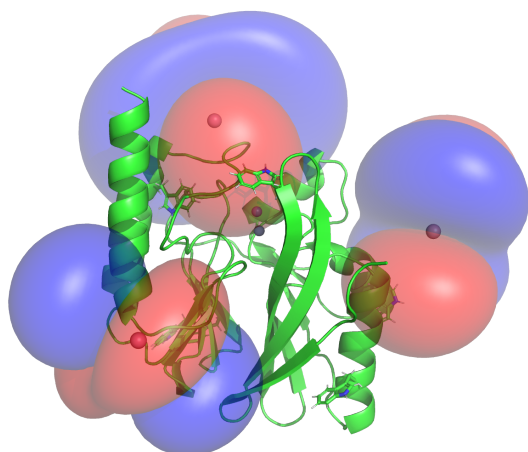
423 None of the minor additional cross-peaks observed in any of the sample preparations
424 could be attributed to alternative conformations of Trp28 either. In particular, the most extreme
425 conformation observed in the crystal structure 1DDK (green in Fig. 1) predicts PCSs > 1 ppm
426 for Trp28 H^{ε1} in the mutant N172C with C2 tags, but we observed no PCS of this magnitude
427 for any of the unassigned peaks.

428
429

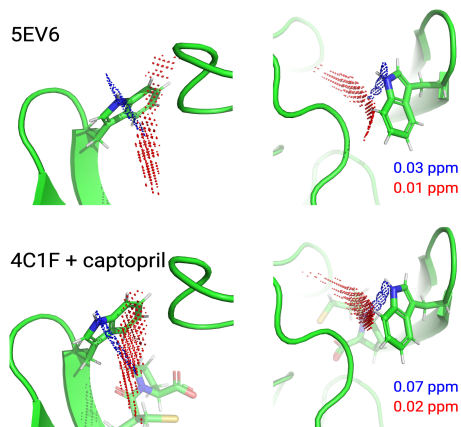
430 **3.4 Defining the localisation space with one versus two lanthanoid ions in the same tag** 431 **and at the same site**

432 Unexpectedly, determining separate localisation spaces from the Tm³⁺ and Tb³⁺ datasets
433 yielded more plausible results than when both datasets were used simultaneously. Careful
434 inspection showed that the close alignment of the Δχ tensors of the Tm³⁺ and Tb³⁺ data resulted
435 in particularly shallow intersection angles of the respective PCS isosurfaces. In calculating the
436 localisation space of Trp28, the PCS isosurfaces arising from the N172C mutant carried by far
437 the greatest weight as this site is closer to residue 28 than the sites 53 and 204. Therefore, the
438 Tm³⁺ and Tb³⁺ data from the N172C mutant dominated the PCS RMSD calculation and the
439 intersection between the associated isosurfaces pulled the final localisation space to a
440 structurally implausible location, which was unstable with respect to small perturbations in Δχ-
441 tensor orientations associated with the tensors at site 172. In contrast, considering the Tm³⁺ and
442 Tb³⁺ datasets separately allowed the localisation spaces to be determined by the intersections
443 with PCS isosurfaces from the other sites. The resulting localisation spaces consistently were
444 compatible with crystal structures.

445



446
 447 **Figure 5.** PCS isosurfaces of the IMP-1 mutants A53C, N172C and S204C plotted on the
 448 crystal structure 5EV6. The respective $\Delta\chi$ tensors were determined from the ^1H PCSs measured
 449 of backbone amides. Blue/red isosurfaces correspond to PCSs of +/-1.0 ppm, respectively,
 450 generated with C2-Tb $^{3+}$ tags.
 451



452
 453 **Figure 6.** Localisation space of the sidechain of Trp28 defined by the PCSs from tags in the
 454 IMP-1 mutants A53C, N172C and S204C. The left and right panels display the same results in
 455 two different orientations. Red and blue points outline localisation spaces determined for the
 456 H $^{\text{C}2}$ and H $^{\text{E}1}$ atoms, respectively. The localisation space of the H $^{\text{C}2}$ atom was defined by the
 457 PCSs and $\Delta\chi$ tensors determined for the Tb $^{3+}$ -loaded C2 tags, while the localisation space of
 458 the H $^{\text{E}1}$ atom was restricted by additional data obtained with C12-Tb $^{3+}$ tag at site N172C. The

459 boundaries of the respective localisation spaces displayed are defined by the PCS RMSD values
460 indicated in ppm. The top panel depicts the localisation spaces determined for the free protein
461 plotted on chain A of the crystal structure 5EV6 depicted in two different orientations. The
462 lower panel depicts the localisation spaces determined in the presence of captopril plotted on
463 chain A of the crystal structure 4C1F.

464

465 3.5 L3 loop conformation in the presence of L-captopril

466 Figure 6 shows that, within the uncertainty of the experiments, the localisation space of the
467 indole sidechain of Trp28 is invariant with respect to the presence or absence of captopril.
468 Conservation of the L3 loop conformation with and without inhibitor is supported by the close
469 similarity in all the PCSs observed for Trp28 in the NOE-relayed [¹³C,¹H]-HSQC spectra (Fig.
470 2 and 3). In the [¹H,¹⁵N]-HSQC spectra of the mutant N172C with C2 tag, however, the PCSs
471 observed for Trp28 H^{ε1} appeared somewhat smaller without than with captopril (Fig. S5b). As
472 the PCSs of backbone amides were very similar in the absence and presence of the inhibitor
473 (Fig. S12), this difference in PCS suggests a change in L3 loop conformation, ~~contradicting the~~
474 ~~observations made with~~ the selectively ¹³C-labelled samples. As discussed above, using the
475 smaller PCS of Trp28 H^{ε1} did not sufficiently change its localisation space in the free protein
476 to render it incompatible with the coordinates of the structure 5EV6. ~~Therefore, as far as the~~
477 ~~data of the ¹⁵N-labelled samples indicate a~~ conformational change of the L3 loop between the
478 free and bound state, ~~it is small. We attribute the differences in PCSs observed between the~~
479 ~~selectively ¹³C-labelled and uniformly ¹⁵N-labelled samples to differences in sample~~
480 ~~preparation of unknown origin, which are also reflected by different numbers of weak~~
481 ~~unassigned cross-peaks (Figs 2, 3, S5 and S6).~~

482 The cross-peak intensities of the Trp28 sidechain resonances are relatively weak
483 compared with those of the other tryptophan sidechains, suggesting that Trp28 is subject to
484 dynamics that broaden its resonances. Its cross-peaks appeared slightly weaker in the presence
485 than in the absence of inhibitor (Fig. 2 and 3), suggesting a change in dynamics caused by the
486 inhibitor binding. Previous NMR studies of metallo-β-lactamases reported faster $R_2(^{15}\text{N})$
487 relaxation rates of the L3-loop tryptophan sidechain in the presence than in the absence of
488 inhibitor, which was attributed to dampened dynamics (Huntley et al., 2000; Softley et al.,
489 2020). In the presence of dynamics, the localisation spaces determined in the present work
490 must be considered averages that do not report on the amplitude or direction of motions.

491

Deleted: 1

Deleted: that did not arise in

Deleted: We therefore have little evidence for a significant

Formatted: Superscript

Formatted: Superscript

495 **3.6 Localisation spaces of tryptophan side chains other than Trp28**

496 As the tagging sites had been designed to analyse the conformation of the L3 loop, they were
497 positioned at similar distances from the L3 loop and therefore not optimal for determining
498 localisation spaces of the other tryptophan residues. Nonetheless, clear differences were
499 observed in the PCSs of the H^{ε2} and H^{ε1} atoms (Fig. 2), allowing the separation of the respective
500 localisation spaces, which also proved to be in excellent agreement with the conformations of
501 the side-chain indoles of Trp62, Trp124 and Trp147 as found in the crystal structure (Fig. S15),
502 whereas the data were insufficient to determine the sidechain conformation of Trp176.

Deleted: 4

503

504 **4 Discussion**

505 The L3 loop of metallo-β-lactamases is known to be flexible and, in the specific case of IMP-
506 1, significantly assists in substrate binding and enzymatic activity (Moali et al., 2003). As the
507 substrate is sandwiched between the di-zinc site and the L3 loop, it is tempting to think that the
508 loop opens up for substrate binding and product release while it may be closed during the
509 enzymatic reaction to hold the substrate and reaction intermediate in place. In contrast, some
510 of the conformations observed in crystal structures of IMP-1 obtained in the presence and
511 absence of the inhibitor L-captopril, revealed the loop in almost identical conformations (Brem
512 et al., 2016). This observation is inconclusive, however, as the L3 loop forms more extensive
513 intermolecular contacts with neighbouring protein molecules in the crystal lattice than
514 intramolecular contacts. In addition, other crystal structures observed the loop to move by
515 almost 3 Å in response to a different inhibitor (Concha et al., 2000). This prompted us to probe
516 its actual location in the absence of crystal packing forces in solution, a task which is difficult
517 to tackle by traditional NMR spectroscopic methods that rely on short-range NOEs.

518 Our results show that by furnishing IMP-1 with paramagnetic lanthanoid tags, the
519 coordinates of the indole sidechain of Trp28, which is a key residue near the tip of the loop,
520 can be determined with remarkable accuracy even in the free protein, where the available
521 crystal structures position the L3 loop in a conformation without any direct contacts with the
522 core of the protein. Indeed, the localisation space identified by the NMR data of the free protein
523 proved to be sufficiently well-defined to discriminate between different crystal structures of
524 IMP-1, as well as between different chains in the same asymmetric crystal unit. For example,
525 the sidechain orientation of Trp28 observed in [Fe³⁺,Zn²⁺]-IMP-1 (4UAM; Carruthers et al.,
526 2014) proved to be in poor agreement with the PCS data, whereas the data were in full
527 agreement with chain A in the structure 5EV6 of [Zn²⁺,Zn²⁺]-IMP-1 without inhibitor

529 (Hinchliffe et al., 2016) and chain A in the structure 4C1F with bound L-captopril (Brem et al.,
530 2016). This highlights the outstanding capacity of PCSs to assess small conformational
531 differences.

532 The approach of using PCSs for local structure determination is particularly appealing
533 in the case of difficult proteins such as IMP-1, where the sequence-specific NMR resonance
534 assignments are incomplete due to line-broadening attributable to motions in the μs – ms time
535 range and additional signals are observed that either stem from protein degradation, misfolding
536 or alternative conformations in slow exchange with the main structure. Notably, all information
537 required to establish the $\Delta\chi$ tensors could be obtained from resolved cross-peaks observed in
538 sensitive $[\text{}^{15}\text{N}, \text{}^1\text{H}]$ -HSQC spectra. Similarly, the localisation information of the tryptophan
539 sidechains could be obtained from sensitive ^{13}C - ^1H and ^{15}N - ^1H correlation spectra. Positioning
540 the lanthanoid tags relatively far from the substrate binding site avoided direct interference
541 with the binding loop structure.

542 In the face of additional signals from minor species, site-selective ^{13}C -labelling of the
543 tryptophan sidechains was particularly helpful for simplifying the $[\text{}^{13}\text{C}, \text{}^1\text{H}]$ -HSQC spectra.
544 Gratifyingly, this could be achieved by providing suitably labelled indole without having to
545 synthesise the full amino acid (Maleckis et al., 2021).

546 It has been pointed out previously that the accuracy with which localisation spaces can
547 be determined is best when PCS isosurfaces intersect in an orthogonal manner (Pintacuda et
548 al., 2006; Lescanne et al., 2018; Zimmermann et al., 2019). In the present work, we found that,
549 counterintuitively, the provision of additional data can considerably degrade the accuracy of
550 the localisation space. This effect arises when PCS isosurfaces intersect at a shallow angle, as
551 the location of these intersections becomes very sensitive with regard to small errors in the
552 relative orientations of the underpinning $\Delta\chi$ tensors. Shallow intersection angles of PCS
553 isosurfaces are common, when two PCS datasets are from tags and tagging sites that differ only
554 in the identity of the paramagnetic metal ion in the tag. This situation commonly generates $\Delta\chi$
555 tensors of different magnitude and sign, but closely similar orientation (Bertini et al., 2001; Su
556 et al., 2008; Keizers et al., 2008; Man et al., 2010; Graham et al., 2011; Joss et al., 2018;
557 Zimmermann et al., 2021). Therefore, while the use of Tm^{3+} and Tb^{3+} tags is helpful for
558 assigning the cross-peaks in the paramagnetic state, more robust results are obtained by using
559 only one of these data sets for calculating the localisation space. Good localisation spaces were
560 thus obtained by using only PCSs measured for Tb^{3+} tags (Fig. 6) or only PCSs measured for
561 Tm^{3+} tags (Fig. S13). In contrast, however, very different tags attached at the same site, such

Deleted: 2

563 as the C2 and C12 tags installed in the mutant N172C, produced independent $\Delta\chi$ -tensor
564 orientations and therefore contributed positively to localising the Trp28 H^{ε1} atom.

565 In principle it is inappropriate to explain a set of PCSs by a single $\Delta\chi$ tensor, if they are
566 generated by a lanthanoid tag attached via a flexible linker, which positions the lanthanide ions
567 at variable coordinates relative to the protein. In this situation, fitting a single $\Delta\chi$ tensor
568 amounts to an approximation. The effective $\Delta\chi$ tensors obtained in this way, however, can
569 fulfill the PCSs remarkably well (Shishmarev and Otting, 2013), as illustrated by the low Q
570 factors obtained in this work (Fig. 4), and the localisation spaces obtained for the tryptophan
571 sidechains are correspondingly well defined.

572 The present work employed ¹H PCSs only, although PCSs were also observed in the
573 indirect dimensions of the [¹³C,¹H]-HSQC and [¹⁵N,¹H]-HSQC spectra. We made this choice
574 because the paramagnetic tags give rise to weak molecular alignments in the magnetic field,
575 which result in residual anisotropic chemical shifts (RACS). The effect is unimportant for ¹H
576 spins but significant for nuclear spins with large chemical shift anisotropy (CSA) tensors such
577 as backbone nitrogens and aromatic carbons. Correcting for the RACS effect is possible with
578 prior knowledge of the CSA tensors and bond orientations (John et al., 2005). We therefore
579 chose not to measure PCSs of the heteronuclear spins in favour of improving sensitivity by
580 accepting a lower spectral resolution in the indirect dimensions.

581 Finally, the C12 tag was designed specifically with the intent to produce a more rigid
582 tether to the protein than the C2 tag, but this did not result in larger $\Delta\chi$ tensors (Table S7) and
583 the NMR spectra of IMP-1 N172C displayed more heterogeneity with the C12 than the C2 tag,
584 suggesting that the shorter and more rigid tether combined with the fairly high molecular
585 weight of the cyclen-lanthanoid complex may have perturbed the protein structure to some
586 degree.

587

588 **5 Conclusion**

589 The current work illustrates how $\Delta\chi$ tensors from paramagnetic lanthanoid ion tags installed at
590 three different sites of the protein can be used to probe the conformation of a selected site in
591 solution in unprecedented detail, provided the structure of most of the protein is known with
592 high accuracy to allow fitting effective $\Delta\chi$ tensors of high predictive value. Importantly,
593 however, the method is easily compromised, if two PCS isosurfaces intersect at a shallow angle
594 as, in this situation, inaccuracies in $\Delta\chi$ tensor determinations have an outsized effect on
595 positioning the localisation spaces defined by the PCSs. Therefore, improved results were

596 obtained by not combining data from different metal ions bound to otherwise identical tags and
597 tagging sites. In the present work, simplifying the NMR spectrum of tryptophan residues by
598 site-selective isotope labelling proved to be of great value for sufficiently improving the
599 spectral resolution to allow assigning the labelled resonances solely from PCSs and PREs. The
600 strategy opens a path to detailed structural investigations of proteins of limited stability like
601 IMP-1, for which complete assignments of the NMR spectrum are difficult to obtain.

602

603

604 **Code and data availability.** NMR spectra and pulse programs are available at
605 <https://doi.org/10.5281/zenodo.5518294>. The script for calculating localisation spaces is
606 available at <https://doi.org/10.5281/zenodo.3594568> and from the GitHub site of Paramagpy.

607

608 **Supplement.** The supplement related to this article is available online at: <https://doi.org/...>

609

610 **Author contributions.** GO initiated the project and edited the final version of the manuscript.
611 HWO wrote NMR pulse programs and software to calculate localisation spaces and performed
612 the $\Delta\chi$ tensor and structure analysis. IDH made labelled protein samples, recorded and assigned
613 NMR spectra, measured PCSs and wrote the first version of the manuscript. AM synthesised
614 the isotope-labelled indole. SJ made ^{15}N -labelled protein mutants with C2 tags and assigned
615 PCSs of backbone amides. MS synthesized C2 tags with different lanthanoid ions. CB, LT and
616 SB synthesized C12 tags with different lanthanoid ions.

617

618 **Competing interests.** The authors declare that they have no conflict of interest.

619

620 **Financial support.** GO thanks the Australian Research Council for a Laureate Fellowship
621 (grant no. FL170100019) and project funding through the Centre of Excellence for Innovations
622 in Peptide and Protein Science, Australian Research Council (grant no. CE200100012). AM
623 thanks the European Regional Development Fund (ERDF) for funding (PostDoc project
624 No. [1.1.1.2/VIAA/2/18/381](https://doi.org/10.1016/j.viaa.2018.03.001)).

625

626 **References**

627 Arakawa, Y., Murakami, M., Suzuki, K., Ito, H., Wacharotayankun, R., Ohsuka, S., Kato, N.,
628 and Ohta, M.: A novel integron-like element carrying the metallo- β -lactamase gene *bla*_{IMP},

629 Antimicrob. Agents Chemother., 39, 1612–1615, <https://doi.org/10.1128/AAC.39.7.1612>,
630 1995.

631 Bertini, I., Janik, M. B. L., Lee, Y. M., Luchinat, C., and Rosato, A.: Magnetic susceptibility
632 tensor anisotropies for a lanthanide ion series in a fixed protein matrix, *J. Am. Chem. Soc.*,
633 123, 4181–4188, <https://doi.org/10.1021/ja0028626>, 2001.

634 Brem, J., van Berkel, S. S., Zollman, D., Lee, S. Y., Gileadi, O., McHugh, P. J., Walsh, T. R.,
635 McDonough, M.A., and Schofield, C. J.: Structural basis of metallo- β -lactamase inhibition
636 by captopril stereoisomers, *Antimicrob. Agents Chemother.*, 60, 142–150,
637 <https://doi.org/10.1128/AAC.01335-15>, 2016.

638 Brewer, K. D., Bacaj, T., Cavalli, A., Camilloni, C., Swarbrick, J. D., Liu, J., Zhou, A., Zhou,
639 P., Barlow, N., Xu, J., Seven, A. B., Prinslow, E. A., Voleti, R., Häussinger, D., Bonvin, A.
640 M. J. J., Tomchick, D. R., Vendruscolo, M., Graham, B., Südhof, T. C., and Rizo, J.:
641 Dynamic binding mode of a synaptotagmin-1-SNARE complex in solution, *Nat. Struct.*
642 *Mol. Biol.*, 22, 555–564, <https://doi.org/10.1038/nsmb.3035>, 2015.

643 Bush, K.: Proliferation and significance of clinically relevant β -lactamases, *Ann. N. Y. Acad.*
644 *Sci.*, 1277, 84–90, <https://doi.org/10.1111/nyas.12023>, 2013.

645 Bush, K.: Alarming β -lactamase-mediated resistance in multidrug-resistant
646 *Enterobacteriaceae*, *Curr. Opin. Microbiol.*, 13, 558–564,
647 <https://doi.org/10.1016/j.mib.2010.09.006>, 2010.

648 Carruthers, T. J.: Paramagnetism & Structural Biology: Biochemical & Biophysical Analysis
649 of IMP-1 Metallo- β -lactamase, PhD thesis, The Australian National University, Canberra,
650 221 pp., 2014.

651 Carruthers, T. J., Carr, P. D., Loh, C.-T., Jackson, C. J., and Otting, G.: Fe^{3+} located in the
652 dinuclear metallo- β -lactamase IMP-1 by pseudocontact shifts, *Angew. Chemie Int. Ed.*, 53,
653 14269–14272, <https://doi.org/10.1002/anie.201408693>, 2014.

654 Chen, W.-N., Nitsche, C., Pilla, K. B., Graham, B., Huber, T., Klein, C. D., and Otting, G.:
655 Sensitive NMR approach for determining the binding mode of tightly binding ligand
656 molecules to protein targets, *J. Am. Chem. Soc.*, 138, 4539–4546,
657 <https://doi.org/10.1021/jacs.6b00416>, 2016.

658 Concha, N. O., Rasmussen, B. A., Bush, K., and Herzberg, O.: Crystal structure of the wide-
659 spectrum binuclear zinc β -lactamase from *Bacteroides fragilis*, *Structure*, 4, 823–836,
660 [https://doi.org/10.1016/S0969-2126\(96\)00089-5](https://doi.org/10.1016/S0969-2126(96)00089-5), 1996.

Deleted: .

662 Concha, N. O., Janson, C. A., Rowling, P., Pearson, S., Cheever, C. A., Clarke, B. P., Lewis,
663 C., Galleni, M., Frere, J.-M., Payne, D. J., Bateson, J. H., and Abdel-Meguid, S. S.: Crystal
664 Structure of the IMP-1 metallo- β -lactamase from *Pseudomonas aeruginosa* and its complex
665 with a mercaptocarboxylate inhibitor: binding determinants of a potent, broad-spectrum
666 inhibitor, *Biochemistry*, 39, 4288–4298, <https://doi.org/10.1021/bi992569m>, 2000.

667 Crick, D. J., Wang, J. X., Graham, B., Swarbrick, J. D., Mott, H. R., and Nietlispach, D.:
668 Integral membrane protein structure determination using pseudocontact shifts, *J. Biomol.*
669 *NMR*, 61, 197–207, <https://doi.org/10.1007/s10858-015-9899-6>, 2015.

670 de la Cruz, L., Nguyen, T.H.D., Ozawa, K., Shin, J., Graham, B., Huber, T., and Otting, G.:
671 Binding of low-molecular weight inhibitors promotes large conformational changes in the
672 dengue virus NS2B-NS3 protease: fold analysis by pseudocontact shifts, *J. Am. Chem. Soc.*,
673 133, 19205–19215, <https://doi.org/10.1021/ja208435s>, 2011.

674 Galleni, M., Lamotte-Brasseur, J., Rossolini, G. M., Spencer, J., Dideberg, O., Frère, J.-M.,
675 and The Metallo- β -Lactamase Working Group: Standard numbering scheme for class B β -
676 lactamases. *Antimicrob. Agents Chemother.*, 45, 660–663,
677 <https://doi.org/10.1128/AAC.45.3.660-663.2001>, 2001.

678 Gianquinto, E., Tondi, D., D'Arrigo, G., Lazzarato, L., and Spyraakis, F.: Can we exploit β -
679 lactamases intrinsic dynamics for designing more effective inhibitors? *Antibiotics*, 9, 833,
680 <https://doi.org/10.3390/antibiotics9110833>, 2020.

681 González, M. M., Abriata, L. A., Tomatis, P. E., and Vila, A. J.: Optimization of
682 conformational dynamics in an epistatic evolutionary trajectory, *Mol. Biol. Evol.*, 33, 1768–
683 1776, <https://doi.org/10.1093/molbev/msw052>, 2016.

684 Graham, B., Loh, C.T., Swarbrick, J.D., Ung, P., Shin, J., Yagi, H., Jia, X., Chhabra, S.,
685 Pintacuda, G., Huber, T., and Otting, G.: A DOTA-amide lanthanide tag for reliable
686 generation of pseudocontact shifts in protein NMR spectra, *Bioconjugate Chem.*, 22, 2118–
687 2125, <https://doi.org/10.1021/bc200353c>, 2011.

688 Guan, J. Y., Keizers, P. H. J., Liu, W. M., Löhr, F., Skinner, S. P., Heeneman, E. A., Schwalbe,
689 H., Ubbink, M., and Siegal, G.: Small-molecule binding sites on proteins established by
690 paramagnetic NMR spectroscopy. *J. Am. Chem. Soc.*, 135, 5859–5868,
691 <https://doi.org/10.1021/ja401323m>, 2013.

692 Herath, I. D., Breen, C., Hewitt, S. H., Berki, T. R., Kassir, A. F., Dodson, C., Judd, M., Jabar,
693 S., Cox, N., Otting, G., and Butler, S. J.: A chiral lanthanide tag for stable and rigid
694 attachment to single cysteine residues in proteins for NMR, EPR and time-resolved

695 luminescence studies, Chem. Eur. J., 27, 13009–13023,
696 <https://doi.org/10.1002/chem.202101143>, 2021.

697 Hinchliffe, P., González, M. M., Mojica, M. F., González, J. M., Castillo, V., Saiz, C.,
698 Kosmopoulou, M., Tooke, C. L., Llarrull, L. I., Mahler, G., and Bonomo, R. A.: Cross-class
699 metallo- β -lactamase inhibition by bisthiazolidines reveals multiple binding modes, Proc.
700 Nat. Acad. Sci., 113, E3745–E3754, <https://doi.org/10.1073/pnas.1601368113>, 2016.

701 Hinchliffe, P., Tanner, C. A., Krismanich, A. P., Labbé, G., Goodfellow, V. J., Marrone, L.,
702 Desoky, A. Y., Calvopiña, K., Whittle, E. E., Zeng, F., and Avison, M. B.: Structural and
703 kinetic studies of the potent inhibition of metallo- β -lactamases by 6-
704 phosphonomethylpyridine-2-carboxylates, Biochemistry, 57, 1880–1892,
705 <https://doi.org/10.1021/acs.biochem.7b01299>, 2018.

706 Hiraiwa, Y., Saito, J., Watanabe, T., Yamada, M., Morinaka, A., Fukushima, T., and Kudo, T.:
707 X-ray crystallographic analysis of IMP-1 metallo- β -lactamase complexed with a 3-
708 aminophthalic acid derivative, structure-based drug design, and synthesis of 3,6-
709 disubstituted phthalic acid derivative inhibitors, Bioorg. Med. Chem. Lett., 24, 4891–4894,
710 <https://doi.org/10.1016/j.bmcl.2014.08.039>, 2014.

711 Huntley, J.J.A., Scrofani, S.D.B., Osborne, M.J., Wright, P.E., and Dyson, H.J.: Dynamics of
712 the metallo- β -lactamase from *Bacteroides fragilis* in the presence and absence of a tight-
713 binding inhibitor, Biochemistry, 39, 13356–13364, <https://doi.org/10.1021/bi001210r>,
714 2000.

715 Huntley, J. J. A., Fast, W., Benkovic, S. J., Wright, P. E., and Dyson, H. J.: Role of a solvent-
716 exposed tryptophan in the recognition and binding of antibiotic substrates for a metallo- β -
717 lactamase, Protein Sci., 12, 1368–1375, <https://doi.org/10.1110/ps.0305303>, 2003.

718 Ito, H., Arakawa, Y., Ohsuka, S., Wachorotayankun, R., Kato, N., and Ohta, M.: Plasmid-
719 mediated dissemination of the metallo- β -lactamase gene *bla_{IMP}* among clinically isolated
720 strains of *Serratia marcescens*, Antimicrob. Agents Chemother., 39, 824–829,
721 <https://doi.org/10.1128/AAC.39.4.824>, 1995.

722 John, M., Park, A. Y., Pintacuda, G., Dixon, N. E., and Otting, G.: Weak alignment of
723 paramagnetic proteins warrants correction for residual CSA effects in measurements of
724 pseudocontact shifts, J. Am. Chem. Soc., 127, 17190–17191,
725 <https://doi.org/10.1021/ja0564259>, 2005.

726 John, M., Park, A. Y., Pintacuda, G., Dixon, N. E., and Otting, G.: Weak alignment of
727 paramagnetic proteins warrants correction for residual CSA effects in measurements of

728 pseudocontact shifts, *J. Am. Chem. Soc.*, 127, 17190–17191,
729 <https://doi.org/10.1021/ja0564259>, 2005.

730 Joss, D., Walliser, R. M., Zimmermann, K., and Häussinger, D.: Conformationally locked
731 lanthanide chelating tags for convenient pseudocontact shift protein nuclear magnetic
732 resonance spectroscopy, *J. Biomol. NMR*, 72, 29–38, [https://doi.org/10.1007/s10858-018-](https://doi.org/10.1007/s10858-018-0203-4)
733 [0203-4](https://doi.org/10.1007/s10858-018-0203-4), 2018.

734 Keizers, P. H. J., Saragliadis, A., Hiruma, Y., Overhand, M., and Ubbink, M.: Design,
735 synthesis, and evaluation of a lanthanide chelating protein probe: CLaNP-5 yields
736 predictable paramagnetic effects independent of environment, *J. Am. Chem. Soc.*, 130,
737 14802–14812, <https://doi.org/10.1021/ja8054832>, 2008.

738 Keizers, P. H. J., Mersinli, B., Reinle, W., Donauer, J., Hiruma, Y., Hannemann, F., Overhand,
739 M., Bernhardt, R., and Ubbink, M.: A solution model of the complex formed by adrenodoxin
740 and adrenodoxin reductase determined by paramagnetic NMR spectroscopy, *Biochemistry*,
741 49, 6846–6855, <https://doi.org/10.1021/bi100598f>, 2010.

742 Kobashigawa, Y., Saio, T., Ushio, M., Sekiguchi, M., Yokochi, M., Ogura, K., and Inagaki, F.:
743 Convenient method for resolving degeneracies due to symmetry of the magnetic
744 susceptibility tensor and its application to pseudo contact shift-based protein-protein
745 complex structure determination, *J. Biomol. NMR*, 53, 53–63,
746 <https://doi.org/10.1007/s10858-012-9623-8>, 2012.

747 Laraki, N., Galleni, M., Thamm, I., Riccio, M. L., Amicosante, G., Frère, J.-M., and Rossolini,
748 G. M.: Structure of In101, a *bla*_{IMP}-containing *Pseudomonas aeruginosa* integron
749 phylogenically related to In5, which carries an unusual array of gene cassettes, *Antimicrob.*
750 *Agents Chemother.*, 43, 890–901, <https://doi.org/10.1128/AAC.43.4.890>, 1999a.

751 Laraki, N., Franceschini, N., Rossolini, G. M., Santucci, P., Meunier, C., De Pauw, E.,
752 Amicosante, G., Frère, J.-M., and Galleni, M.: Biochemical characterization of the
753 *Pseudomonas aeruginosa* 101/1477 metallo-β-lactamase IMP-1 produced by *Escherichia*
754 *coli*, *Antimicrob. Agents Chemother.*, 43, 902–906, <https://doi.org/10.1128/AAC.43.4.902>,
755 1999b.

756 Lescanne, M., Ahuja, P., Blok, A., Timmer, M., Akerud, T., and Ubbink, M.: Methyl group
757 reorientation under ligand binding probed by pseudocontact shifts, *J. Biomol. NMR*, 71,
758 275–285, <https://doi.org/10.1007/s10858-018-0190-5>, 2018.

759 Linciano, P., Cendron, L., Gianquinto, E., Spyarakis, F., and Tondi, D.: Ten years with New
760 Delhi metallo- β -lactamase-1 (NDM-1): from structural insights to inhibitor design, ACS
761 Infect. Dis. 5, 9–34, <https://doi.org/10.1021/acsinfecdis.8b00247>, 2018.

762 Maleckis, A., Herath, I. D., and Otting, G.: Synthesis of $^{13}\text{C}/^{19}\text{F}/^2\text{H}$ labeled indoles for use as
763 tryptophan precursors for protein NMR spectroscopy, Org. Biomol. Chem., 19, 5133–5147,
764 <https://doi.org/10.1039/D1OB00611H>, 2021.

765 Man, B., Su, X.-C., Liang, H., Simonsen, S., Huber, T., Messerle, B. A., and Otting, G.: 3-
766 Mercapto-2,6-pyridinedicarboxylic acid, a small lanthanide-binding tag for protein studies
767 by NMR spectroscopy, Chem. Eur. J., 16, 3827–3832,
768 <https://doi.org/10.1002/chem.200902904>, 2010.

769 Markley, J. L., Bax, A., Arata, Y., Hilbers, C. W., Kaptein, R., Sykes, B. D., Wright, P. E., and
770 Wüthrich, K.: Recommendations for the presentation of NMR structures of proteins and
771 nucleic acids - IUPAC-IUBMB-IUPAB Inter-Union Task Group on the Standardization of
772 Data Bases of Protein and Nucleic Acid Structures Determined by NMR Spectroscopy, J.
773 Biomol. NMR, 12, 1–23, <https://doi.org/10.1023/A:1008290618449>, 1998.

774 Meissner, A., Duus, J. Ø., and Sørensen, O. W.: Spin-state-selective excitation. Application for
775 E.COSY-type measurement of J_{HH} coupling constants, J. Magn. Reson., 128, 92–97,
776 <https://doi.org/10.1006/jmre.1997.1213>, 1997.

777 Moali, C., Anne, C., Lamotte-Brasseur, J., Gros Lambert, S., Devreese, B., Van Beeumen, J.,
778 Galleni, M., and Frère, J.M.: Analysis of the importance of the metallo- β -lactamase active
779 site loop in substrate binding and catalysis, Chemistry & Biology, 10, 319–329,
780 [https://doi.org/10.1016/S1074-5521\(03\)00070-X](https://doi.org/10.1016/S1074-5521(03)00070-X), 2003.

781 Orton, H. W., Huber, T., and Otting, G.: Paramagpy: software for fitting magnetic
782 susceptibility tensors using paramagnetic effects measured in NMR spectra, Magn.
783 Reson., 1, 1–12, <https://doi.org/10.5194/mr-1-1-2020>, 2020.

784 Palacios, A. R., Mojica, M. F., Giannini, E., Taracila, M. A., Bethel, C. R., Alzari, P. M., Otero,
785 L. H., Klinke, S., Llarrull, L. I., Bonomo, R. A., and Vila, A. J.: The reaction mechanism of
786 metallo- β -lactamases is tuned by the conformation of an active-site mobile loop,
787 Antimicrob. Agents Chemother, 63, e01754-18, <https://doi.org/10.1128/AAC.01754-18>,
788 2019.

789 Payne, D. J., Hueso-Rodriguez, J. A., Boyd, H., Concha, N. O., Janson, C. A., Gilpin, M.,
790 Bateson, J. H., Cheever, C., Niconovich, N. L., Pearson, S., Rittenhouse, S., Tew, D., Díez,
791 E., Pérez, P., de la Fuente, J., Rees, M., and Rivera-Sagredo, A.: Identification of a series of

792 tricyclic natural products as potent broad-spectrum inhibitors of metallo- β -lactamases,
793 *Antimicrob. Agents Chemother.*, 46, 1880–1886, [https://doi.org/10.1128/AAC.46.6.1880-](https://doi.org/10.1128/AAC.46.6.1880-1886.2002)
794 [1886.2002](https://doi.org/10.1128/AAC.46.6.1880-1886.2002), 2002.

795 Pearce, B. J. G., Jabar, S., Loh, C. T., Szabo, M., Graham, B., and Otting, G.: Structure
796 restraints from heteronuclear pseudocontact shifts generated by lanthanide tags at two
797 different sites, *J. Biomol. NMR*, 68, 19–32, <https://doi.org/10.1007/s10858-017-0111-z>,
798 2017.

799 Pilla, K. B., Otting, G., and Huber, T.: Protein structure determination by assembling super-
800 secondary structure motifs using pseudocontact shifts, *Structure*, 25, 559–568,
801 <https://doi.org/10.1016/j.str.2017.01.011>, 2017.

802 Pintacuda, G., Park, A. Y., Keniry, M. A., Dixon, N. E., and Otting, G.: Lanthanide labeling
803 offers fast NMR approach to 3D structure determinations of protein-protein complexes, *J.*
804 *Am. Chem. Soc.*, 128, 3696–3702, <https://doi.org/10.1021/ja057008z>, 2006.

805 Rossi, M.-A., Martinez, V., Hinchliffe, P., Mojica, M. F., Castillo, V., Moreno, D. M., Smith,
806 R., Spellberg, B., Drusano, G. L., Banchio, C., Bonomo, R. A., Spencer, J., Vila, A. J., and
807 Mahler, G.: 2-Mercaptomethyl-thiazolidines use conserved aromatic-S interactions to
808 achieve broad-range inhibition of metallo- β -lactamases, *Chem. Sci.*, 12, 2898–2908,
809 <https://doi.org/10.1039/d0sc05172a>, 2021.

810 Salimraj, R., Hinchliffe, P., Kosmopoulou, M., Tyrrell, J. M., Brem, J., van Berkel, S. S.,
811 Verma, A., Owens, R. J., McDonough, M. A., Walsh, T. R., Schofield, C. J., and Spencer,
812 J.: Crystal structures of VIM-1 complexes explain active site heterogeneity in VIM-class
813 metallo- β -lactamases, *FEBS J.*, 286, 169–183, <https://doi.org/10.1111/febs.14695>, 2018.

814 Shishmarev, D. and Otting, G.: How reliable are pseudocontact shifts induced in proteins and
815 ligands by mobile paramagnetic metal tags? A modelling study, *J. Biomol. NMR*, 56, 203–
816 216, <https://doi.org/10.1007/s10858-013-9738-6>, 2013.

817 Softley, C. A., Zak, K. M., Bostock, M. J., Fino, R., Zhou, R. X., Kolonko, M., Mejd-Nitiu,
818 R., Meyer, H., Sattler, M., and Popowicz, G. M.: Structure and molecular recognition
819 mechanism of IMP-13 metallo- β -lactamase, *Antimicrob. Agents Chemother.*, 64, e00123-
820 20, <https://doi.org/10.1128/AAC.00123-20>, 2020.

821 Su, X.-C., McAndrew, K., Huber, T., and Otting, G.: Lanthanide-binding peptides for NMR
822 measurements of residual dipolar couplings and paramagnetic effects from multiple angles,
823 *J. Am. Chem. Soc.*, 130, 1681–1687, <https://doi.org/10.1021/ja076564l>, 2008.

824 Toney, J. H., Hammond, G. G., Fitzgerald, P. M., Sharma, N., Balkovec, J. M., Rouen, G. P.,
825 Olson, S. H., Hammond, M. L., Greenlee, M. L., and Gao, Y. D.: Succinic acids as potent
826 inhibitors of plasmid-borne IMP-1 metallo- β -lactamase, *J. Biol. Chem.*, 276, 31913–31918,
827 <https://doi.org/10.1074/jbc.M104742200>, 2001.

828 van Duin, D., Kaye, K. S., Neuner, E. A., and Bonomo, R. A.: Carbapenem-resistant
829 Enterobacteriaceae: a review of treatment and outcomes, *Diagn. Microbiol. Infect. Dis.* 75,
830 115–120, <https://doi.org/10.1016/j.diagmicrobio.2012.11.009>, 2013.

831 Wachino, J., Kanechi, R., Nishino, E., Mochizuki, M., Jin, W., Kimura, K., Kurosaki, H., and
832 Arakawa, Y.: 4-Amino-2-sulfanylbenzoic acid as a potent subclass B3 metallo- β -lactamase-
833 specific inhibitor applicable for distinguishing metallo- β -lactamase subclasses, *Antimicrob.*
834 *Agents Chemother.* 63, e01197-19, <https://doi.org/10.1128/AAC.01197-19>, 2019.

835 Watanabe, M., S. Iyobe, M. Inoue, and S. Mitsunashi: Transferable imipenem resistance in
836 *Pseudomonas aeruginosa*, *Antimicrob. Agents Chemother.* 35, 147–151, [https://doi.org/](https://doi.org/10.1128/AAC.35.1.147)
837 [10.1128/AAC.35.1.147](https://doi.org/10.1128/AAC.35.1.147), <https://doi.org/10.1128/AAC.35.1.147>, 1991.

838 Yagi, H., Pilla, K. B., Maleckis, A., Graham, B., Huber, T., and Otting, G.: Three-dimensional
839 protein fold determination from backbone amide pseudocontact shifts generated by
840 lanthanide tags at multiple sites, *Structure*, 21, 883–890,
841 <https://doi.org/10.1016/j.str.2013.04.001>, 2013.

842 Yamaguchi, Y., Matsueda, S., Matsunaga, K., Takashio, N., Toma-Fukai, S., Yamagata, Y.,
843 Shibata, N., Wachino, J., Shibayama, K., Arakawa, Y., and Kurosaki, H.: Crystal structure
844 of IMP-2 metallo- β -lactamase from *Acinetobacter* spp.: comparison of active-site loop
845 structures between IMP-1 and IMP-2, *Biol. Pharm. Bull.* 38, 96–
846 101, <https://doi.org/10.1248/bpb.b14-00594>, 2015.

847 Yamaguchi, Y., Kato, K., Ichimaru, Y., Jin, W., Sakai, M., Abe, M., Wachino, J., Arakawa,
848 Y., Miyagi, Y., Imai, M., Fukuishi, N., Yamagata, Y., Otsuka, M., Fujita, M., and Kurosaki,
849 H.: Crystal structures of metallo- β -lactamase (IMP-1) and its D120E mutant in complexes
850 with citrate and the inhibitory effect of the benzyl group in citrate monobenzyl ester, *J. Med.*
851 *Chem.*, 64, 10019–10026, <https://doi.org/10.1021/acs.jmedchem.1c00308>, 2021.

852 Yamaguchi, H., M. Nukaya, and T. Sawai, T: Sequence of *Klebsiella pneumoniae* RDK4
853 metallo- β -lactamase, EMBO database accession no. D29636, EMBO, Heidelberg,
854 Germany, 1994.

855 Zimmermann, K., Joss, D., Müntener, T., Nogueira, E. S., Schäfer, M., Knörr, L., Monnard,
856 F. W., and Häussinger, D.: Localization of ligands within human carbonic anhydrase II

857 using ^{19}F pseudocontact shift analysis, *Chem. Sci.*, 10, 5064–5072,
858 <https://doi.org/10.1039/c8sc05683h>, 2019.